

**Determination of  $^{59}\text{Ni}(n, xp)$  reaction cross sections using surrogate reactions**

Jyoti Pandey,<sup>1</sup> Bhawna Pandey,<sup>1,\*</sup> A. Pal,<sup>2,3</sup> S. V. Suryanarayana,<sup>2</sup> S. Santra,<sup>2,3</sup> B. K. Nayak,<sup>2,3</sup> E. T. Mirgule,<sup>2</sup> Alok Saxena,<sup>2</sup> D. Chattopadhyay,<sup>2,3</sup> A. Kundu,<sup>2,3</sup> V. V. Desai,<sup>2,†</sup> A. Parihari,<sup>2,4</sup> G. Mohanto,<sup>2</sup> D. Sarkar,<sup>2</sup> P. C. Rout,<sup>2,3</sup> B. Srinivasan,<sup>2</sup> K. Mahata,<sup>2,3</sup> B. J. Roy,<sup>2,3</sup> S. De,<sup>2</sup> and H. M. Agrawal<sup>1</sup>

<sup>1</sup>*Department of Physics, G.B. Pant University of Agriculture and Technology, Pantnagar, Uttarakhand 263 145, India*

<sup>2</sup>*Nuclear Physics Division, Bhabha Atomic Research Centre, Mumbai 400 085, India*

<sup>3</sup>*Homi Bhabha National Institute, Anushaktinagar, Mumbai 400 094, India*

<sup>4</sup>*Department of Physics, University of Mumbai, Mumbai 400 098, India*



(Received 27 October 2017; revised manuscript received 19 November 2018; published 14 January 2019)

The  $^{59}\text{Ni}(n, xp)$  reaction cross sections have been measured following the surrogate reaction ratio method in the equivalent neutron energy range of 11.9–15.8 MeV by populating the compound nucleus  $^{60}\text{Ni}^*$  through transfer reaction  $^{56}\text{Fe}(^6\text{Li}, d)$  at  $E_{\text{lab}} = 35.9$  MeV. The  $^{59}\text{Co}(^6\text{Li}, \alpha)^{61}\text{Ni}^*$  transfer reaction at  $E_{\text{lab}} = 40.5$  MeV has been used as the reference reaction which is the surrogate of  $^{60}\text{Ni}(n, xp)$  reaction populating the compound nucleus  $^{61}\text{Ni}^*$ . The proton decay probabilities have been determined by measuring evaporated protons at backward angles in coincidence with projectile like fragments (PLFs, either  $d$  or  $\alpha$ ) detected around grazing angles. The cross sections for the reference reaction  $^{60}\text{Ni}(n, xp)$  are taken from JENDL-4.0 library, which closely reproduce the available experimental data. The cross sections for the desired  $^{59}\text{Ni}(n, xp)$  reaction so obtained compare well with the nuclear-reactions-model code TALYS-1.8 using microscopic level densities. The present experimental data are consistent with the evaluated data library of ROSFOND-2015 but not with TENDL-2015 and ENDF/B-VIII, indicating the need of new evaluations for this reaction of importance to fusion technology.

DOI: [10.1103/PhysRevC.99.014611](https://doi.org/10.1103/PhysRevC.99.014611)

**I. INTRODUCTION**

High quality data on nuclear structure and reactions are essential components for simulation of reactor behavior in nominal, incidental, and accidental conditions and also to predict the running conditions of nuclear energy systems. Recent investigations on the impact of nuclear data uncertainties on performance characteristics of systems considered for waste transmutation, Generation-IV reactors and fusion reactors (ITER) show that the accuracy and completeness of existing nuclear data are important issues for the safety assessment of the present day as well as the upcoming innovative nuclear energy systems for fission and fusion technologies [1,2].

Out of the many neutron induced reactions that take place inside a fusion reactor, the ones that produce gaseous elements like hydrogen and helium are of utmost importance for the study of structural integrity of reactor materials. The production of hydrogen and helium gases takes place mainly through  $(n, xp)$  and  $(n, x\alpha)$  reactions. These reactions are induced on the first wall, structural and blanket materials of the fusion reactor. In addition to the production of hydrogen and helium, the other processes such as atomic displacements and transmutations can produce microstructural defects and modify physical properties of the materials [3]. The materials

suitable for the reactor structures are stainless steel with Cr, Fe, and Ni as main constituents (in SS316 content of Fe  $\approx$  65%, Ni  $\approx$  12%, Cr  $\approx$  17%). Natural nickel contains five stable isotopes, i.e.,  $^{58,60,61,62,64}\text{Ni}$ . The  $^{59}\text{Ni}$  nuclide, a long-lived radioisotope of nickel ( $T_{1/2} = 7.6 \times 10^4$  year), is produced during the reactor operation via the major pathways  $^{58}\text{Ni}(n, \gamma)^{59}\text{Ni}$  and  $^{60}\text{Ni}(n, 2n)^{59}\text{Ni}$  [4], with natural abundances of  $^{58}\text{Ni}$  and  $^{60}\text{Ni}$  of 68.077% and 26.223%, respectively. The reactions  $^{59}\text{Ni}(n, xp)$  and  $^{59}\text{Ni}(n, x\alpha)$  involving the long-lived radioisotope  $^{59}\text{Ni}$  are also the sources of helium and hydrogen production [5,6]. The  $^{59}\text{Ni}$  isotope participates in three highly exothermic reactions such as  $(n, \gamma)$ ,  $(n, p)$ , and  $(n, \alpha)$  with  $Q$  values of 11.387, 1.855, and 5.096 MeV, respectively. These reactions contribute to the displacement and radiation damage and are receiving renewed attention for the study of helium and hydrogen production in fusion reactor materials. In a fusion reactor, the neutron spectrum contains a significant thermal component, and  $^{58}\text{Ni}$  has a substantial  $(n, \gamma)$  cross section ( $\approx 4$  b [7]) for thermal neutrons. Thus, when the reactor is in operation,  $^{58}\text{Ni}$  gets rapidly converted to  $^{59}\text{Ni}$ . Again,  $^{59}\text{Ni}$  has large thermal  $(n, \alpha)$  ( $\approx 7.38$ – $22.3$  b) and  $(n, p)$  ( $\approx 1.4$ – $4.0$  b) cross sections [8–10] with large positive  $Q$  values. The rapid ingrowth of  $^{59}\text{Ni}$  leads to an enhanced production of hydrogen and helium in a nonlinear fashion. So far, neutron induced reactions on  $^{59}\text{Ni}$  at nonthermal energies have not been studied for the production of hydrogen in fusion reactor materials [11–14]. Therefore, it is important to measure the cross sections for the  $(n, p)$  as well as the total proton emission  $(n, xp)$  channels of the long-lived isotope

\*bhawna.16p@gmail.com

<sup>†</sup>Present address: Department of Chemistry, Oregon State University, Corvallis, Oregon 97331 USA.

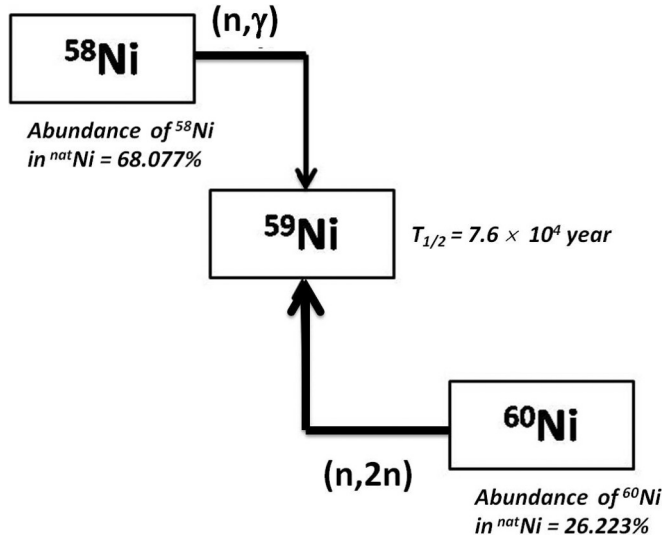


FIG. 1. Schematic of  $^{59}\text{Ni}$  formation pathways in a typical fusion reactor.

$^{59}\text{Ni}$  [15,16], for which data are not available in EXFOR libraries. Various evaluated data libraries also show large discrepancies [17–19]. These long-lived radionuclides also contribute to nuclear waste and radiation damage safety issue, as they have significant neutron induced cross sections in the neutron energy range starting from threshold up to 20 MeV. The major pathways that produce  $^{59}\text{Ni}$  from the stable Ni isotopes present in structural material are shown in Fig. 1.

Direct experimental measurements of cross sections for unstable long-lived radionuclide ( $^{59}\text{Ni}$ ) are not possible as it does not occur in naturally available Ni isotopes. In the present work, we determine the  $^{59}\text{Ni}(n, xp)$  cross sections using surrogate reactions. In a surrogate reaction, the residual compound nucleus is populated over a wide range of excitation energy. Therefore, with a fixed beam energy, the surrogate method allows one to determine the cross sections over a wide range of equivalent neutron energies [20]. The evaluated cross sections of the  $^{60}\text{Ni}(n, xp)$  reaction as a function of excitation energy obtained from JENDL-4.0 have been used as the reference to determine the  $^{59}\text{Ni}(n, xp)$  cross sections from the measured ratio of the proton decay probabilities of  $^{60}\text{Ni}^*$  and  $^{61}\text{Ni}^*$  compound systems.

The paper has been organized as follows. The details of the present measurements are described in Sec. II. The key assumptions involved in the nuclear model codes with Hauser-Feshbach statistical model calculations and the optimized input parameters chosen are discussed in Sec. III. The experimental data and their interpretation are discussed in Sec. IV. The results have been summarized in Sec. V.

## II. EXPERIMENTAL DETAILS AND DATA ANALYSIS

Measurements were carried out using  $^6\text{Li}$  beams obtained from the BARC-TIFR Pelletron Accelerator Facility in Mumbai. The self-supporting thin metallic targets of  $^{\text{nat}}\text{Fe}$  (abundance of  $^{56}\text{Fe} \approx 92\%$ ) and  $^{59}\text{Co}$  (abundance  $\approx 100\%$ ) of thickness  $\approx 700 \mu\text{g}/\text{cm}^2$  each prepared by rolling and vacuum

TABLE I. Surrogate reactions investigated in the present experiment, their ground-state  $Q$  values ( $Q_{gg}$ ), the compound nucleus (CN) formed, neutron separation energies ( $S_n$ ) and corresponding equivalent neutron induced reactions.

$E_{\text{beam}}^{6\text{Li}}$ (MeV)	Surrogate reaction	$Q_{gg}$ (MeV)	CN	$S_n$ (MeV)	Equivalent neutron induced reaction
35.9	$^{56}\text{Fe}(^6\text{Li}, d)^{60}\text{Ni}^*$	4.817	$^{60}\text{Ni}$	11.387	$^{59}\text{Ni}(n, p)$
40.5	$^{59}\text{Co}(^6\text{Li}, \alpha)^{61}\text{Ni}^*$	13.65	$^{61}\text{Ni}$	7.820	$^{60}\text{Ni}(n, p)$

evaporation techniques, respectively, were bombarded at incident energies of  $E_{\text{lab}} = 35.9$  and  $40.5$  MeV, respectively. The surrogate reactions of our interest, their ground-state  $Q$  values ( $Q_{gg}$ ), neutron separation energies ( $S_n$ ), and corresponding equivalent neutron induced reactions are listed in Table I for the present experiment.

Two  $\Delta E$ - $E$  silicon surface barrier (SSB) detector telescopes (T1 and T2) with  $\Delta E$  detectors of thickness  $150 \mu\text{m}$  and  $100 \mu\text{m}$  and with  $E$  detectors of thickness of  $1 \text{ mm}$  were mounted inside a scattering chamber (of  $1.5$  meter diameter) at angles of  $25^\circ$  and  $35^\circ$  with respect to the beam direction around the transfer grazing angle to identify the projectile-like fragments (PLFs) as shown in Fig. 2. Different PLFs, i.e., proton, deuteron, triton, and  $\alpha$  particles are uniquely identified in two dimensional plot of  $\Delta E$  versus the total energy ( $E_{\text{tot}}$ ). This plot is converted into an effective particle identification (PI) versus total energy plot. A linearization function  $\text{PI} = b(E_{\text{tot}}^{1.70} - E_{\text{res}}^{1.70})$  was used to generate the PI curve, where  $E_{\text{tot}}$  is the total particle energy,  $E_{\text{res}}$  is the energy deposited in the  $E$  detector, and  $b$  is a constant. The spectra obtained from telescopes (T1 and T2) as well as strip telescopes (S1 and S2) have been energy calibrated using the known energies of (i)  $\alpha$  particles from a Pu-Am  $\alpha$  source and (ii) the excited states of  $^{16}\text{O}^*$  formed in an in-beam experiment

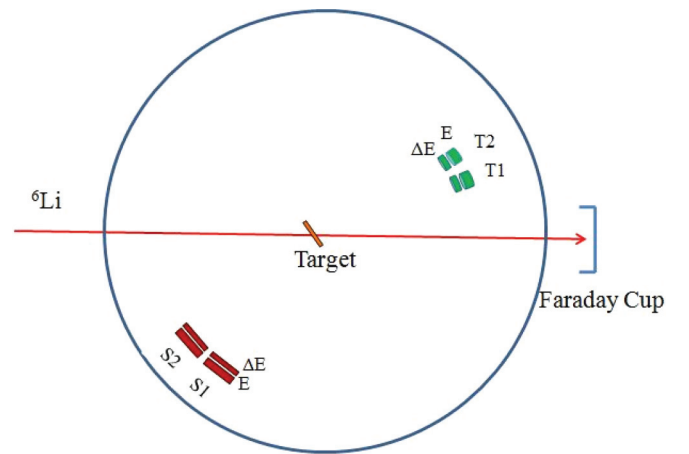


FIG. 2. A schematic diagram of experimental setup inside a  $1.5\text{-m}$ -diameter scattering chamber. Here, T1 and T2 are particle telescopes for detecting the projectile like fragments (PLFs) placed at a distance of about  $17 \text{ cm}$  from the target center. The strip telescopes S1 and S2 have been used to identify the evaporated particles like proton and  $\alpha$  and placed at about the same distance as T1 and T2.

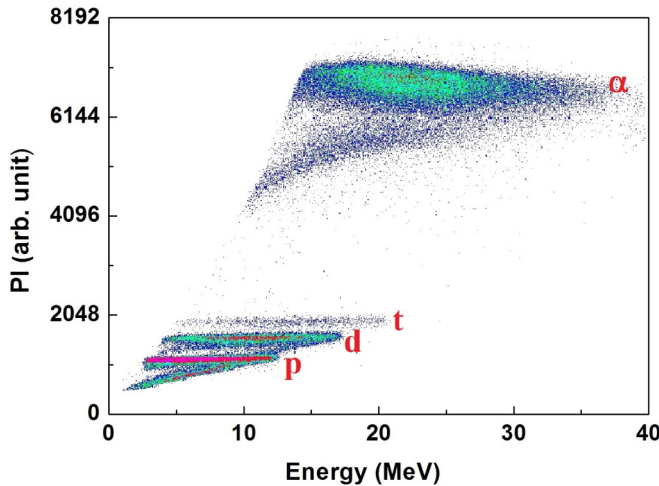


FIG. 3. A typical plot of particle identification (PI) versus total energy ( $E_{\text{tot}}$ ) of the PLFs produced in  $^6\text{Li} + ^{56}\text{Fe}$  reaction at  $E_{\text{lab}} = 35.89$  MeV, measured in T1.

on the  $^{12}\text{C}(^6\text{Li}, d)^{16}\text{O}^*$  reaction at 18 MeV. A typical PI versus total energy plot obtained from T1 telescope is shown in Fig. 3, where all PLFs are clearly identified. The events in which the compound nuclei  $^{60}\text{Ni}^*$  and  $^{61}\text{Ni}^*$  are formed in  $^{56}\text{Fe}(^6\text{Li}, d)^{60}\text{Ni}^*$  and  $^{59}\text{Co}(^6\text{Li}, \alpha)^{61}\text{Ni}^*$  transfer reactions are identified by detecting the evaporating protons by strip detectors in coincidence with the outgoing  $d$  and  $\alpha$  PLFs by single telescopes, respectively.

Two large area Si strip telescopes (S1 and S2) have been placed at backward angles covering the angular ranges of  $110^\circ$ – $130^\circ$  and  $140^\circ$ – $160^\circ$  (see Fig. 2), to detect the evaporated particles (e.g.,  $p$ ,  $d$ ,  $t$ , and  $\alpha$ ) from the compound nuclei  $^{60}\text{Ni}^*$  and  $^{61}\text{Ni}^*$  in coincidence with the PLFs (detected in T1 and T2). Each strip telescope consists of two Si strip detectors placed back to back ( $\Delta E$ - $E$ ) with active area  $\approx 50$  mm  $\times$  50 mm. Each detector has 16 vertical strips of size 3.1 mm  $\times$  50.0 mm and thickness of  $\Delta E \approx 60$   $\mu\text{m}$  and  $E \approx 1500$   $\mu\text{m}$ . A typical two dimensional  $\Delta E$  versus  $E_{\text{tot}}$  spectrum obtained from one of the 32  $\Delta E$ - $E$  strip combinations has been shown in Fig. 4, which clearly shows the mass discrimination for H isotopes ( $p$ ,  $d$ ,  $t$ ) and  $^4\text{He}$ . The time correlations between the projectile-like fragments (PLF) detected in T1 or T2 and the decay particles detected in strip detectors S1 or S2 were recorded through a time to amplitude converter (TAC). A typical two-dimensional plot of ‘TAC’ versus ‘PLF deuteron energy’ measured by T1 for  $^6\text{Li} + ^{56}\text{Fe}$  reaction at  $E_{\text{lab}} = 35.9$  MeV is shown in Fig. 5. The outgoing evaporated proton spectra from the compound system  $^{60}\text{Ni}^*$  in coincidence with projectile-like fragment deuteron is shown in Fig. 6. In this spectrum, the deuteron energies were selected around the peak values of deuteron PLF energies ( $E_d = 11.5$ – $12.5$  MeV) in each of the single telescopes T1 and T2, which correspond to equivalent neutron energy of neutron induced reaction of  $E_n \approx 14$  MeV and the compound nucleus excitation energy  $\approx 25.2$  MeV. The statistical model calculations using PACE4 [21] were carried out

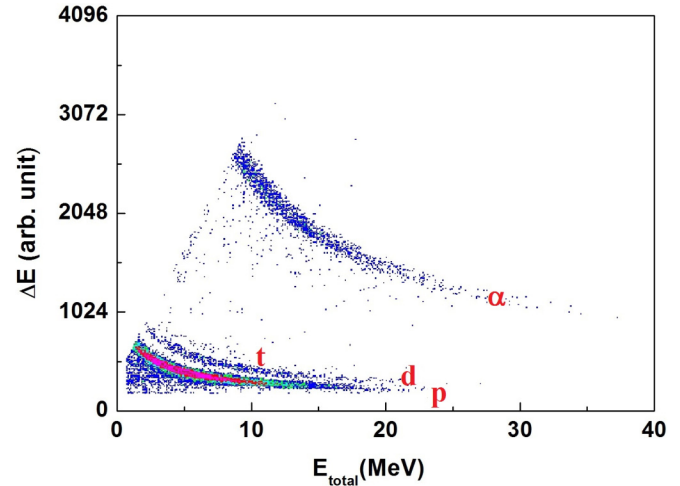


FIG. 4. A typical two-dimensional  $\Delta E$  versus  $E_{\text{tot}}$  spectrum obtained from one of the 32  $\Delta E$ - $E$  strip combinations placed at backward angles, for  $^6\text{Li} + ^{56}\text{Fe}$  reaction at  $E_{\text{lab}} = 35.89$  MeV.

to estimate the proton spectrum evaporated from the same compound nucleus at the excitation energy corresponding to 14 MeV incident neutrons. As shown in Fig. 6, the predictions of PACE4 calculations and experimental proton spectra compare well, indicating the compound nuclear nature of the emitted protons.

It may be worth mentioning that the contributions of pre-equilibrium emission of protons for the desired reaction and the reference reaction have been estimated using TALYS-1.8 code and found to be negligible (less than 2% and 5%, respectively) in the energy range of the present measurements. The calculated cross sections for pre-equilibrium proton emission along with the ones for direct, compound nucleus evaporation and total proton emissions are shown in Fig. 7 for reactions induced by (a)  $\alpha$  transfer, i.e., the surrogate of  $^{60}\text{Ni}(n, xp)$  reaction and (b) deuteron transfer, i.e., the surrogate of  $^{59}\text{Ni}(n, xp)$  reaction, respectively.

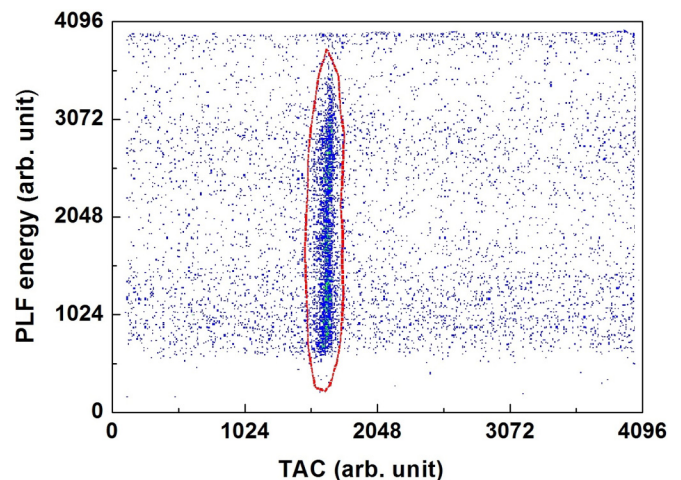


FIG. 5. A typical PLF -proton TAC versus deuteron (PLF) energy plot in the  $^6\text{Li} + ^{56}\text{Fe}$  reactions at  $E_{\text{lab}} = 35.9$  MeV.

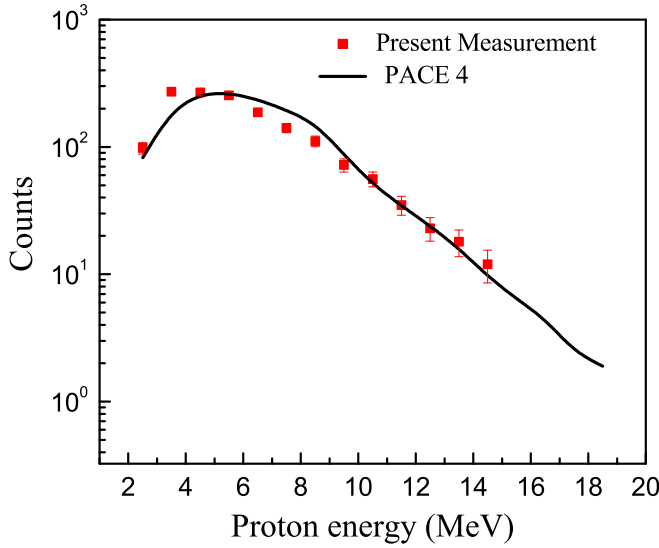


FIG. 6. Measured proton energy spectra in coincidence with deuteron PLFs for the  ${}^6\text{Li} + {}^{56}\text{Fe}$  reaction at 35.89 MeV corresponding to a compound nucleus excitation energy of  $\approx 25$  MeV. The statistical model prediction by PACE4 normalized to the data is shown as a continuous line.

The compound systems  ${}^{60}\text{Ni}^*$  and  ${}^{61}\text{Ni}^*$  are found to be populated at overlapping excitation energies in the range of  $\approx 22$ – $32$  MeV in  ${}^{56}\text{Fe}({}^6\text{Li}, d){}^{60}\text{Ni}^*$  reaction at  $E_{\text{lab}}({}^6\text{Li}) = 35.89$  MeV and  ${}^{59}\text{Co}({}^6\text{Li}, \alpha){}^{61}\text{Ni}^*$  reaction at  $E_{\text{lab}}({}^6\text{Li}) = 40.5$  MeV, respectively. The proton decay probabilities of  ${}^{60}\text{Ni}^*$  and  ${}^{61}\text{Ni}^*$  compound nuclei produced in the transfer reactions are obtained using the following relation:

$$\Gamma_p^{CN}(E^*) = \frac{1}{\epsilon_s} \frac{N_{ip}(E^*)}{N_i(E^*)}. \quad (1)$$

The subscript ‘ $i$ ’ in Eq. (1) denotes either deuteron or  $\alpha$  PLF channel corresponding to the  ${}^{60}\text{Ni}^*$  or  ${}^{61}\text{Ni}^*$  compound nucleus.  $N_i$  and  $N_{ip}$  denote the singles and coincidence counts, respectively, at excitation energy  $E^*$ . The efficiency of the

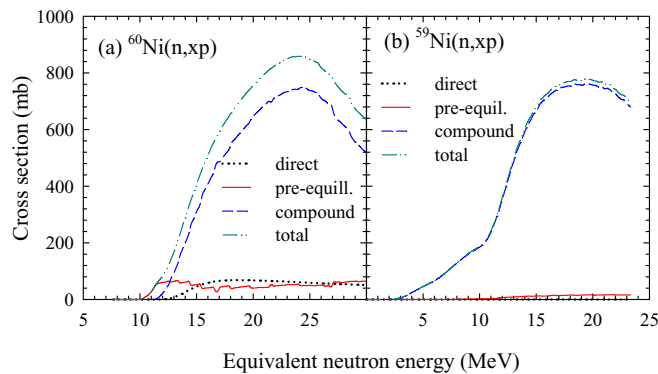


FIG. 7. A comparison of proton emission cross sections, estimated using TALYS-1.8, for pre-equilibrium, direct, compound nucleus, and total production in case of two different reactions, i.e., (a)  $\alpha$  transfer and (b) deuteron transfer reactions, respectively. The ‘‘direct’’ production in the second case is very small and cannot be seen above the x axis.

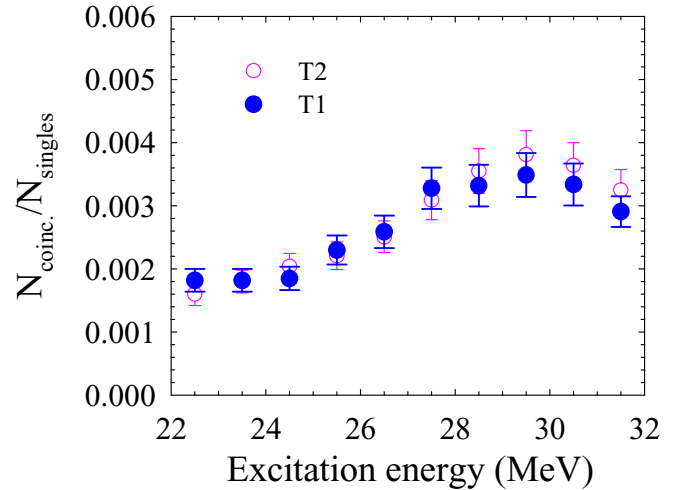


FIG. 8. Ratio of proton counts in coincidence to singles as a function of excitation energy of the composite nucleus  ${}^{60}\text{Ni}^*$  obtained using the gate of the PLF telescopes (a) T1 and (b) T2.

strip detectors to detect the evaporated protons in coincidence with PLFs is taken to be  $\epsilon_s$ .

The excitation energy spectra of target-like residues of  ${}^{60}\text{Ni}^*$  and  ${}^{61}\text{Ni}^*$  were determined on an event by event mode by employing two-body kinematics for deuteron and  $\alpha$  PLF channels. Since the PLF telescopes T1 and T2 are placed at two different angles ( $25^\circ$  and  $35^\circ$ ) to detect the outgoing projectile breakup fragment the angular momentum of the excited compound nucleus formed by the capture of its complementary breakup fragment by the target nucleus may vary

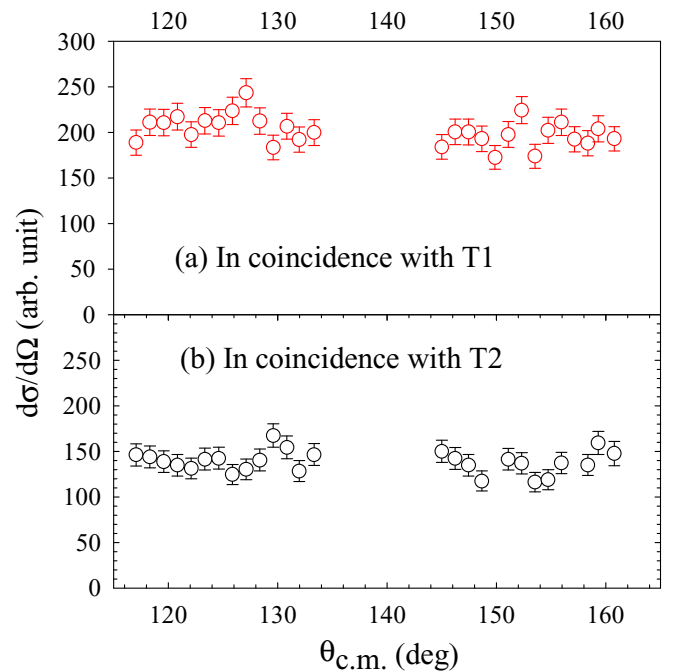


FIG. 9. Angular distributions of protons produced in  ${}^6\text{Li} + {}^{56}\text{Fe}$  system as measured by strip telescopes in coincidence with PLFs detected by (a) T1 and (b) T2.

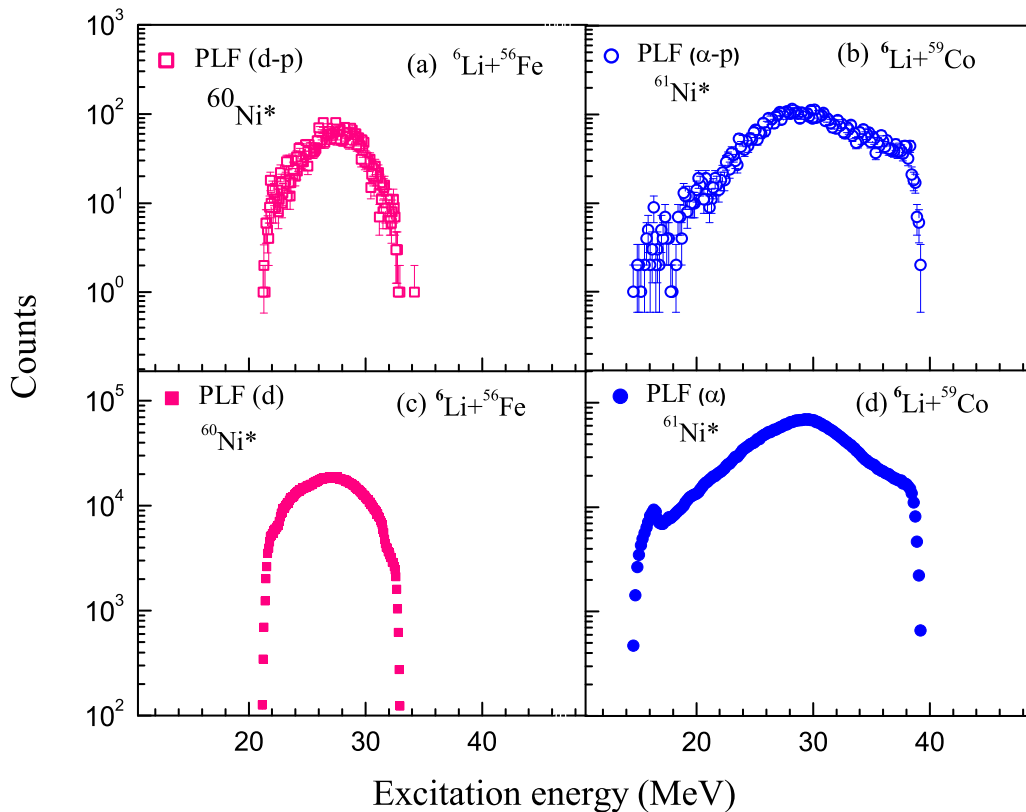


FIG. 10. Excitation energy spectra of the target-like fragments produced in  ${}^6\text{Li} + {}^{56}\text{Fe}$  and  ${}^6\text{Li} + {}^{59}\text{Co}$  reactions corresponding to PLF deuteron and  $\alpha$  respectively with [(a), (b)] and without [(c), (d)] coincidence with evaporated protons.

for the data using T1 from that of T2. In order to investigate the difference, if any, the proton decay probabilities have been obtained separately and shown in Fig. 8 as functions of excitation energy of the composite nucleus  ${}^{60}\text{Ni}^*$ . The comparison shows that the two proton decay probabilities, measured using T1 and T2, are in good agreement in the overlapping excitation energies of our interest. It implies that the effect of angular momentum of the excited compound nucleus on proton decay probabilities that determine the  $(n, xp)$  cross section is negligible.

Further, to investigate the composite nucleus angular momentum dependence on the evaporated proton spectra, the angular distributions of the protons measured by the strip telescopes S1 as well as S2 covering the angular range of  $110^\circ$ – $160^\circ$  have been obtained using the coincidence data separately for T1 and T2 as shown in Figs. 9(a) and 9(b), respectively. The isotropic distribution in both cases suggests that the angular distribution of the evaporated protons is independent of PLF emission angles of T1 and T2. A difference in the counts of two cases observed in two plots is due to the difference in PLF cross sections at  $25^\circ$  (T1) and  $35^\circ$  (T2) as expected. The results of Figs. 8 and 9 confirm the validity of the method used in the present surrogate study.

The results of Fig. 8 suggests that the coincidence data using two PLF telescopes T1 and T2 can be combined to increase the statistics, which has been done here in the following manner. For each of the telescopes the excitation energy of the composite nucleus corresponding to each event has been

evaluated separately using the two-body kinematics. Then, the counts corresponding to the same excitation energy bins generated using T1 and T2 have been added to obtain the final excitation energy spectrum. The excitation energy spectra so obtained for  ${}^{60}\text{Ni}^*$  and  ${}^{61}\text{Ni}^*$  nuclei in coincidence with outgoing PLFs are shown in Figs. 10(a) and 10(b), respectively. The respective excitation energy spectra corresponding to the singles are shown in Figs. 10(c) and 10(d). The proton decay probabilities for the excited compound systems  ${}^{60}\text{Ni}^*$  and  ${}^{61}\text{Ni}^*$  for the desired and reference reactions, respectively, have been calculated in steps of 1 MeV excitation energy using the coincidence and singles counts of the respective reactions in Eq. (1). The proton evaporation cross section of a compound system at a particular excitation energy  $E^*$  is proportional to the product of the above proton decay probability  $\Gamma_p^{\text{CN}}(E^*)$  and the corresponding neutron-induced compound nuclear formation cross-section  $\sigma^{\text{CN}}(E^*)$ . Hence, the ratio of the proton evaporation cross section of  ${}^{60}\text{Ni}^*$  to that of  ${}^{61}\text{Ni}^*$  can be obtained by using the following expression:

$$\frac{\sigma^{59\text{Ni}(n,xp)}(E^*)}{\sigma^{60\text{Ni}(n,xp)}(E^*)} = \frac{\sigma_{n+^{59}\text{Ni}}^{\text{CN}}(E^*) \Gamma_p^{60\text{Ni}}(E^*)}{\sigma_{n+^{60}\text{Ni}}^{\text{CN}}(E^*) \Gamma_p^{61\text{Ni}}(E^*)}. \quad (2)$$

The  ${}^{60}\text{Ni}(n, xp)$  reaction cross-section values as a function of excitation energy were used as the reference reaction cross sections which were obtained from JENDL-4.0 [19] evaluation that closely reproduces the available experimental data taken from EXFOR as shown in Fig. 11. Since, the cross sections

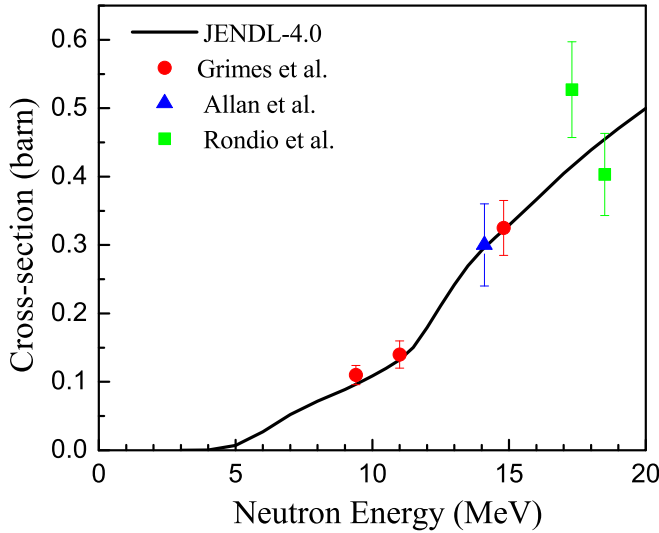


FIG. 11.  $^{60}\text{Ni}(n, xp)$  data from JENDL compared to available experimental data taken from EXFOR.

for  $^{60}\text{Ni}(n, xp)$  reaction were available only up to  $E_n = 20$  MeV [19], corresponding to the  $^{61}\text{Ni}$  excitation energy of 27.5 MeV, the cross sections determined for  $^{59}\text{Ni}(n, xp)$  reaction were restricted to smaller excitation energy range ( $E^* \approx 23.5\text{--}27.5$  MeV).

The cross sections for neutron capture leading to  $^{60}\text{Ni}^*$  and  $^{61}\text{Ni}^*$  compound systems were calculated by TALYS-1.8 code. Using these CN formation cross sections along with the cross section for reference reaction  $^{60}\text{Ni}(n, xp)$  and the measured proton decay probabilities in Eq. (2), the experimental cross sections for  $^{59}\text{Ni}(n, xp)$  have been obtained for the same  $^{60}\text{Ni}^*$  excitation energy range. The above excitation energy range was then converted to equivalent neutron energy range of  $E_n = 11.9\text{--}15.8$  MeV, using the expression “ $E_n = \frac{A+1}{A}(E^* - S_n)$ ”, where  $A + 1 (=60)$  is the mass number and  $S_n (=11.387$  MeV) is the neutron separation energy of the compound nucleus  $^{60}\text{Ni}$ .

### III. NUCLEAR MODEL CALCULATIONS

The TALYS-1.8 code [22] has been used to calculate the total hydrogen production cross section induced by neutrons on the stable isotopes of nickel, i.e.,  $^{58,60,61,62,64}\text{Ni}$ , as well as the radioactive isotopes  $^{59,63}\text{Ni}$ . The hydrogen production cross sections widely differ for each nickel isotope. The  $^{59}\text{Ni}(n, p)$  reaction cross sections ( $\approx 500$  mb at 14 MeV) are comparable to the other stable isotopes of nickel. The reactions  $^{59}\text{Ni}(n, p)$ ,  $^{59}\text{Ni}(n, 2p)$ , and  $^{59}\text{Ni}(n, np)$  have energy thresholds of 0.0, 5.602, 8.745 MeV, respectively. In the present work, we treat the detected protons as  $(n, xp)$  that includes all proton emission channels.

The TALYS-1.8 calculations have been carried out for neutron energy up to 20 MeV within the framework of Hauser-Feshbach statistical model with pre-equilibrium corrections [23]. All the required inputs like nuclear masses, discrete energy levels, transmission coefficients, and nuclear level densities (NLD) of nuclides involved in the calculations have been

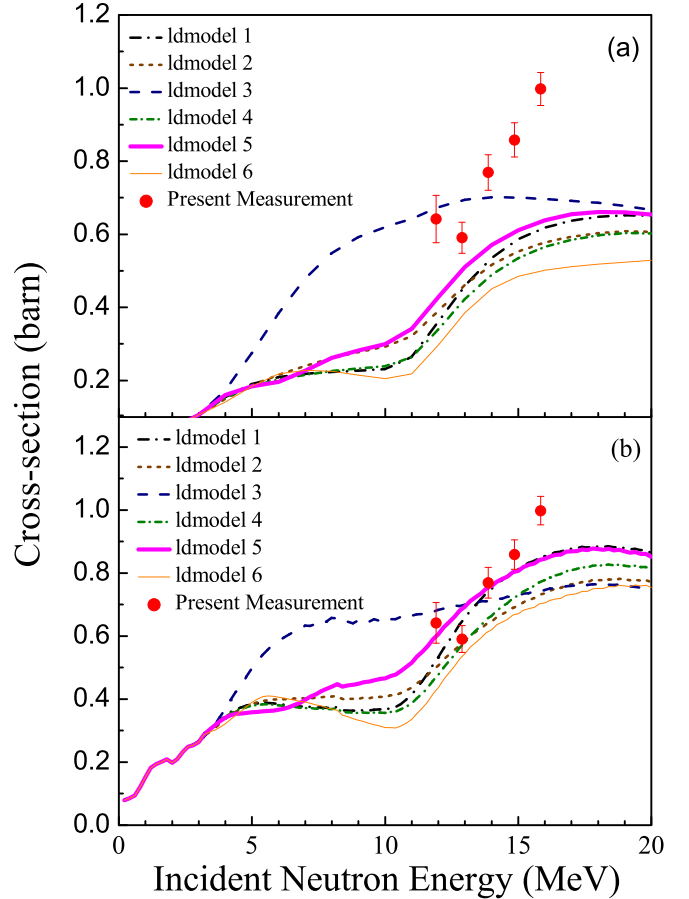


FIG. 12. Experimental cross sections for  $^{59}\text{Ni}(n, xp)$  reactions have been compared with TALYS-1.8 predictions using different level density models with (a) default parameters and (b)  $rv$  adjusted parameters.

taken from the latest reference input parameter library RIPL-3 [24]. The global optical model potentials for neutron and proton proposed by Koning and Delaroche [25] have been used, which are required to calculate the transmission coefficients. Results using different level density models of TALYS-1.8 with default parameters for  $^{59}\text{Ni}(n, xp)$  cross sections are shown in Fig. 12(a), along with the present experimental data (filled circles) for a comparison. It can be seen that the calculation using the option ldmodel-3, that uses phenomenological generalized superfluid model (GSM) [26], gives higher values of cross sections. Whereas, other ldmodel options predict lower cross sections, though the option ldmodel-5 predicts the trend close to the experimental data. Adjustment of model input parameters has improved the agreement with experimental data, as shown in Fig. 12(b) for all ldmodels with optical model potential volume radius parameter  $rv = 1.25$  (TALYS-1.8) for both protons and neutrons. Therefore, we use  $rv$  adjusted ldmodel-5 option for the TALYS calculations as well as the final comparison with the experimental data. The TALYS-1.8 reference input parameter library contains new energy, spin, and parity-dependent nuclear level densities based on the microscopic combinatorial model proposed by Hilaire and Goriely [26]. The calculations make coherent use of nuclear structure properties determined within the deformed Skyrme-

Hartree-Fock-Bogoliubov framework [26] and *ldmodel-5* using the improved level density parameters [27].

The TALYS-1.8 calculations have been performed with *ldmodel-5* option for various values of photon ( $\gamma$ ) strength functions (PSF) covering all the PSF models from 1–8. It has been observed that the predictions for  $(n, \gamma)$  channel depend on the PSF models, however, cross sections for  $^{59}\text{Ni}(n, p)$ ,

$^{59}\text{Ni}(n, 2p)$ ,  $^{59}\text{Ni}(n, np)$  channels are not sensitive to PSF model changes. Therefore, in the present work, we use default value for gamma strength function to compare with the experimental data as discussed in the next section. The contributions of  $(n, p)$ ,  $(n, 2p)$ ,  $(n, np)$  channels for proton emission from various Ni isotopes, formed in the surrogate reaction of  $^6\text{Li}$  induced on natural Fe, are shown in Fig. 13 using *rv* adjusted *ldmodel-5* option. Results show that all the three channels mentioned above contribute to the proton emission in the energy range of our interest. Hence, a combined cross section for  $(n, xp)$  channels has been obtained from the present measurement.

#### IV. RESULTS AND DISCUSSION

The cross sections determined for  $^{59}\text{Ni}(n, xp)$  reactions from the present surrogate measurements have been compared with different nuclear model calculations as well as the evaluated nuclear data libraries like ENDF/B-VIII, ROSFOND-2015, and TENDL-2015 as shown in Fig. 14. Results from TALYS-1.8 code and the evaluations of ROSFOND-2015 are in qualitative agreement with the measured cross sections in the equivalent neutron energy range 11.9–15.8 MeV. The measured  $^{59}\text{Ni}(n, xp)$  reaction cross sections do not agree with evaluated nuclear data libraries such as ENDF/B-VIII and TENDL-2015. In Fig. 14, the enriched curve is obtained from TALYS-1.8 considering only  $^{59}\text{Ni}(n, xp)$  reaction cross sections which corresponds to 100% enriched  $^{56}\text{Fe}$  target. The calculations for natural composition of iron correspond to the inclusion of contributions from  $^{57}\text{Ni}(n, p)$ ,  $^{59}\text{Ni}(n, p)$ ,  $^{60}\text{Ni}(n, p)$ ,  $^{61}\text{Ni}(n, p)$  with appropriate abundances of  $^{\text{nat}}\text{Fe}$  target used in the experiment (having  $^{54}\text{Fe} \approx 5.85\%$ ,  $^{56}\text{Fe} \approx 91.75\%$ ,  $^{57}\text{Fe} \approx 2.12\%$ , and  $^{58}\text{Fe} \approx 0.28\%$ ). Due to the large abundance of  $^{56}\text{Fe}$  in the natural Fe target, the proton emission is found to be dominated by  $^{59}\text{Ni}(n, xp)$  channel among all the  $(n, xp)$  channels of different Ni isotopes (populated by

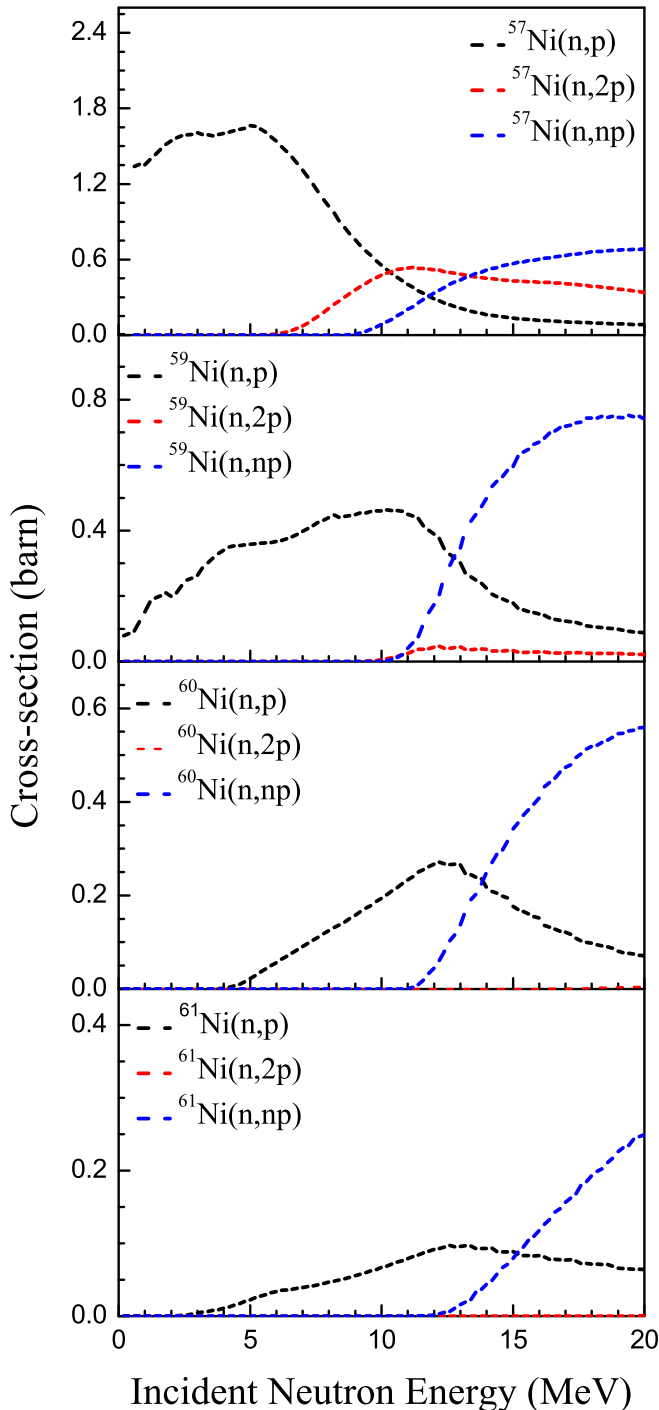


FIG. 13. TALYS-1.8 results for cross sections of  $(n, p)$ ,  $(n, 2p)$ ,  $(n, np)$  components of  $^{57,59,60,61}\text{Ni}(n, xp)$  for *rv* adjusted level density model option 5.

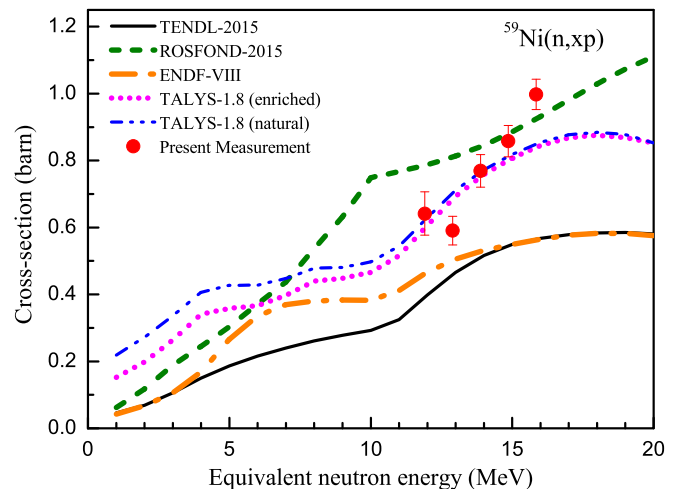


FIG. 14. The  $^{59}\text{Ni}(n, xp)$  cross sections as a function of equivalent neutron energy along with the ones from various nuclear data libraries and TALYS-1.8 nuclear model calculations for the cases of enriched and natural targets as discussed in the text.

${}^6\text{Li}$  induced surrogate reactions on natural Fe). Though, the  $Q$  value for proton emission from  ${}^{57}\text{Ni}(n, p)$  (+4.044 MeV) is larger than for  ${}^{59}\text{Ni}(n, p)$ , the contribution to proton emission is much less due to its low abundance as well as higher neutron energy range considered in the present experiment. However, the large positive  $Q$  value for  ${}^{57}\text{Ni}(n, p)$  reaction increases the proton emission at lower energies as compared to the enriched target case, as shown by deviation of natural and enriched curves at lower neutron energies in Fig. 14.

## V. SUMMARY AND CONCLUSION

In summary, we have deduced the  ${}^{59}\text{Ni}(n, xp)$  cross sections by employing the surrogate ratio method. Protons detected from CN populated by  ${}^{56}\text{Fe}({}^6\text{Li}, d){}^{60}\text{Ni}^*$  and  ${}^{59}\text{Co}({}^6\text{Li}, \alpha){}^{61}\text{Ni}^*$  transfer reactions were used as surrogate of the desired reaction  ${}^{59}\text{Ni}(n, xp)$  and reference reaction  ${}^{60}\text{Ni}(n, xp)$ , respectively. Compound nuclei  ${}^{60}\text{Ni}^*$  and  ${}^{61}\text{Ni}^*$  were populated at overlapping excitation energies, and proton evaporation probabilities were measured in the excitation energy range of  $\approx 22$ – $32$  MeV. The surrogate ratio method has been used to determine the  ${}^{59}\text{Ni}(n, xp)$  cross sections

in the equivalent neutron energy range of 11.9–15.8 MeV by using the reference  ${}^{60}\text{Ni}(n, xp)$  cross sections taken from JENDL-4.0. In the experiment,  ${}^{\text{nat}}\text{Fe}$  target was used. Out of several channels, i.e.,  ${}^{57,59,60,61}\text{Ni}(n, xp)$  reactions, opened by surrogate reactions of natural Fe, the contributions to proton emission are found to be dominated by  ${}^{59}\text{Ni}(n, xp)$  reaction. Measured cross sections of  ${}^{59}\text{Ni}(n, xp)$  reactions compare well with the predictions of nuclear model code TALYS-1.8 for both enriched and natural targets and the ROSFOND-2015 library, but they are higher than the values obtained from ENDF/B-VIII and TENDL-2015 data libraries. The observed discrepancies in different data libraries with the experimental data and theoretical model calculations indicate the need for new evaluations for this reaction.

## ACKNOWLEDGMENTS

Authors acknowledge the financial support provided by Department of Science and Technology under Project No. YSS/2015/001842. We are thankful to BARC-TIFR Pelletron Linac Facility staff for providing uninterrupted beams during the experiment.

- 
- [1] Report summary of European facility for innovative reactor and transmutation neutron data, project report on 2013, Belgium, id:211499, <https://cordis.europa.eu/project/rcn/88553/reporting/en>.
  - [2] ITER Physics Basis Editors, ITER Physics Expert Group Chairs and Co-chairs and ITER Joint Central Team and Physics Integration Unit, *Nucl. Fusion*, **39**, 2137 (1999).
  - [3] M. R. Gilbert, S. Dudarev, S. Zheng, L. W. Packer, and J. Sublet, *Nucl. Fusion* **52**, 083019 (2012).
  - [4] R. A. Forrest, A. Tabasso, C. Danani, S. Jaxhar, and A. K. Shaw, *Handbook of Activation Data Calculated Using EASY-2007* (EURATOM / UKAEA Fusion Association, Culham Science Centre, Abingdon, UK, 2009), p. 552.
  - [5] L. R. Greenwood and F. A. Garner, *J. Nucl. Mater.* **233**, 1530 (1996).
  - [6] H. Iida, V. Khripunov, L. Petrizzi, and G. Federici, Nuclear Analysis Report (NAR), Nuclear Analysis Group, ITER Naka & Garching Joint Work Sites, ITER Report, G 73 DDD 2W 0.2, July 2004.
  - [7] P. Zucec, M. Barbagallo, N. Colonna *et al.*, *Phys. Rev. C* **89**, 014605 (2014).
  - [8] H. M. Eiland and G. J. Kirouac, *Nucl. Sci. Eng.* **53**, 1 (1974).
  - [9] J. McDonald and N. G. Sjostrand, *Atomkernenergie (ATKE) Bd.* **27**, 112 (1976).
  - [10] M. Asghar, A. Emsallem, and N. G. Sjostrand, *Z. Phys. A* **282**, 375 (1977).
  - [11] F. A. Garner, L. R. Greenwood, and B. M. Oliver, Effects of Radiation on Materials: 18th International Symposium, ASTM STP 1325, American Society for Testing and Materials, West Conshohocken, PA, 1999.
  - [12] L. Greenwood and D. Bowers, Presented at Sixth ASTM-Euratom Symposium on Reactor Dosimetry, Jackson Hole, WY, June 1–5, 1987.
  - [13] R. Haight, International Conference on Nuclear Data for Science and Technology, CEA 2007, EDP Sciences, p. 1081, <http://nd2007.edpsciences.org>.
  - [14] R. Haight, Proc. International Conference Nuclear Cross Section for Technology, Oct. 22–26, 1979.
  - [15] R. A. Forrest, *Fusion Eng. Des.* **81**, 2143 (2006).
  - [16] R. A. Forrest, *Energy Procedia* **7**, 540 (2011).
  - [17] EXFOR data library, <https://www-nds.iaea.org/exfor/exfor.htm>.
  - [18] Endf data library, <https://www-nds.iaea.org/exfor/endlf.htm>.
  - [19] EXFOR data library, <https://www.ndc.jaea.go.jp/jendl/j40/j40.html>.
  - [20] B. Pandey, V. V. Desai, S. V. Suryanarayana, B. K. Nayak *et al.*, *Phys. Rev. C* **93**, 021602(R) (2016).
  - [21] A. Gavron, *Phys. Rev. C* **21**, 230 (1980).
  - [22] A. J. Koning, S. Hilaire, and S. Goriely, TALYS-1.8, A Nuclear Reaction Program, User Manual, NRG, Petten, Netherlands (2015), available with TALYS-1.8 code distribution at <https://www.talys.eu>.
  - [23] W. Hauser and H. Feshbach, *Phys. Rev.* **87**, 366 (1952).
  - [24] R. Capote *et al.*, *Nucl. Data Sheets* **110**, 3107 (2009).
  - [25] A. J. Koning and J. P. Delaroche, *Nucl. Phys. A* **713**, 231 (2003).
  - [26] S. Goriely, S. Hilaire, and A. J. Koning, *Phys. Rev. C* **78**, 064307 (2008).
  - [27] S. Hilaire, M. Girod, S. Goriely, and A. J. Koning, *Phys. Rev. C* **86**, 064317 (2012).